Skin Complications of Diabetes Mellitus Revealed by Polarized Hyperspectral Imaging and Machine Learning

Viktor Dremin [ID], Zbignevs Marcinkevics, Evgeny Zherebtsov [ID], Alexey Popov, Andris Grabovskis, Hedviga Kronberga, Kristine Geldnere, Alexander Doronin, Igor Meglinski [ID], *Senior Member, IEEE*, and Alexander Bykov [ID]

Abstract— Aging and diabetes lead to protein glycation and cause dysfunction of collagen-containing tissues. The accompanying structural and functional changes of collagen significantly contribute to the development of various pathological malformations affecting the skin, blood vessels, and nerves, causing a number of complications, increasing disability risks and threat to life. In fact, no methods of non-invasive assessment of glycation and associated metabolic processes in biotissues or prediction of possible skin complications, e.g., ulcers, currently exist for endocrinologists and clinical diagnosis. In this publication, utilizing emerging photonics-based technology, innovative solutions in machine learning, and definitive physiological characteristics, we introduce a diagnostic approach capable of evaluating the skin complications of diabetes mellitus at the very earlier stage. The results of the feasibility studies, as well as the actual tests on patients with diabetes and healthy volunteers, clearly show the ability of the approach to differentiate diabetic and control groups. Furthermore, the developed in-house polarization-based hyperspectral imaging technique accomplished with the implementation of the artificial neural network provides new horizons in the study and diagnosis of age-related diseases.

Index Terms— Hyperspectral imaging, polarization, diabetes mellitus, skin complications.

Viktor Dremin is with the College of Engineering and Physical Sciences, Aston University, Birmingham B4 7ET, U.K., and also with the Opto-Electronics and Measurement Techniques Unit, University of Oulu, 90570 Oulu, Finland (e-mail: v.dremin1@aston.ac.uk).

Zbignevs Marcinkevics is with the Department of Human and Animal Physiology, University of Latvia, LV-1004 Riga, Latvia (e-mail: zbigis@latnet.lv).

Evgeny Zherebtsov and Alexander Bykov are with the Opto-Electronics and Measurement Techniques Unit, University of Oulu, 90570 Oulu, Finland (e-mail: evgenii.zherebtsov@oulu.fi; alexander.bykov@oulu.fi).

Alexey Popov is with the VTT Technical Research Centre of Finland, 90571 Oulu, Finland (e-mail: alexey.popov@vtt.fi).

Andris Grabovskis is with the Biophotonics Laboratory, Institute of Atomic Physics and Spectroscopy, University of Latvia, LV-1004 Riga, Latvia (e-mail: andris.grabovskis@gmail.com).

Hedviga Kronberga is with the Medical Center Plavnieki, LV-1021 Riga, Latvia (e-mail: hedviga.kronberga@gmail.com).

Kristine Geldnere is with the Pauls Stradins Clinical University Hospital, LV-1002 Riga, Latvia (e-mail: kristineab@inbox.lv).

Alexander Doronin is with the Computer Graphics Group, School of Engineering and Computer Science, Victoria University of Wellington, Wellington 6140, New Zealand (e-mail: alex.doronin@vuw.ac.nz).

Igor Meglinski is with the College of Engineering and Physical Sciences, Aston University, Birmingham B4 7ET, U.K., also with the Opto-Electronics and Measurement Techniques Unit, University of Oulu, 90570 Oulu, Finland, also with the Institute of Engineering Physics for Biomedicine (PhysBio), National Research Nuclear University MEPhI (Moscow Engineering Physics Institute), 115409 Moscow, Russia, also with the Interdisciplinary Laboratory of Biophotonics, National Research Tomsk State University, 634050 Tomsk, Russia, and also with the Institute of Clinical Medicine N.V. Sklifosovsky, I.M. Sechenov First Moscow State Medical University, 129090 Moscow, Russia (e-mail: igor.meglinski@oulu.fi).

This article has supplementary downloadable material available at https://doi.org/10.1109/TMI.2021.3049591, provided by the authors.

Digital Object Identifier 10.1109/TMI.2021.3049591

I. INTRODUCTION

ACCORDING to the International Diabetes Federation, the problem of early diagnosis and monitoring the effectiveness of diabetes mellitus (DM) treatment is one of the most acute in modern healthcare. In 2019, there were 463M patients with DM in the world, and by 2045 this figure is to increase to 700M [1]. DM is one of the ten deadliest diseases with a yearly mortality rate of over 1M. Recent studies [1] have demonstrated that timely diagnosis and treatment, including enhancement of the patient control, reduce complications and make it possible to reverse their development if detected at the early preclinical stages.

In people with DM, over time, high blood glucose level (known as hyperglycemia) causes damage to many biological tissues in the body that leads to the development of disability-causing and life-threatening medical complications. One of the consequences of DM is the appearance of foot tissue lesions (diabetic foot syndrome). The main factor in the pathogenesis of foot tissue lesions at DM is a violation of blood microcirculation. Recent studies [2] have revealed that microvascular lesions in various organs, including the feet, are registered already in the first years of diabetes and even at prediabetic conditions long before the clinical manifestations of vascular complications. Therefore, increasing the effectiveness of prevention and treatment of diabetic angiopathies is possible only with timely diagnosis and correction of vascular disorders at early stages. Timely detection of microvascular disorders followed by the appropriate treatment reduces the risk of complications and makes it possible to reverse their

development at the early preclinical stage [3]. The incidence of microangiopathies depends not only on the duration of DM but also on how early the correct diagnosis has been performed as well as on the effectiveness of the treatment. To date, a common disadvantage of the methods available to clinicians for the diagnosis of complications of DM is the inability to noninvasively assess the degree of tissue glycation and monitor its metabolism, as well as to determine the location of skin areas most probably exposed to the development of trophic ulcers. One of the ways to improve the quality of diagnosis in modern medicine and advanced medical/biological research is to use the methods of optical diagnostics, many of which are successfully applied in clinical practice, e.g. microscopy techniques [4], pulse oximetry and photoplethysmography (PPG) [5], optical coherence tomography (OCT) [6], indocyanine green fluorescent imaging [7], etc. The advantages of such techniques are associated with their non-invasiveness, high resolving power, low procedure cost, and high productivity. Using *a priori* data along with the information obtained by non-invasive optical imaging methods, as well as advanced approaches to data mining would allow identifying the patients with an increased risk of diabetic foot syndrome and assessing the areas of the lower extremities most prone to the development of ulcerative defects.

Diffuse reflectance spectroscopy (DRS) has found its application in many areas of medicine [8], including endoscopic diagnosis of cancer [9], [10], cancer surgery [11], dermatology [12], etc. Analysis of the changes in the spectrum of diffuse reflectance of tissues can provide rich information about their physiological and morphological state. DRS technique has been implemented to assess the peripheral blood flow and the oxygen saturation. The method is able to provide continuous non-invasive measurement of oxy- (HbO_2) and deoxyhaemoglobin (Hb) concentrations. By recording a diffuse reflectance spectrum, it is possible to determine the oxygen saturation of the tissue, using the spectrum shape (its slope, area under the curve) on the basis of mathematical simulations of the relation between the reflectance and concentration of the Hb/HbO_2 [13].

Hyperspectral imaging (HSI) is a modern implementation of the DRS method providing information about the tissue functional state. To implement hyperspectral measurements, a series of images of the object under study are registered in narrow wavelength ranges. Analysis of the hyperspectral data allows one to assess the content of the main absorbers in the biological tissue, blood volume, oxygen saturation, etc.

This method is widely used in various medical applications [14], [15]. It is also able to detect systemic and local microcirculatory changes associated with DM [13]. The technology is most commonly used to analyze the development of wounds, including diabetic ulcers, burns [16] and bruises [17]. Studies conducted in DM using HSI technology have shown the ability of the method not only to evaluate the effectiveness of the therapy of diabetic ulcers, but also to predict their development even before they appear [18]–[20]. It was concluded that HSI can accurately predict ulcer healing during a few months and identify ulcers that are at risk of not healing and therefore, could be used to screen for lower
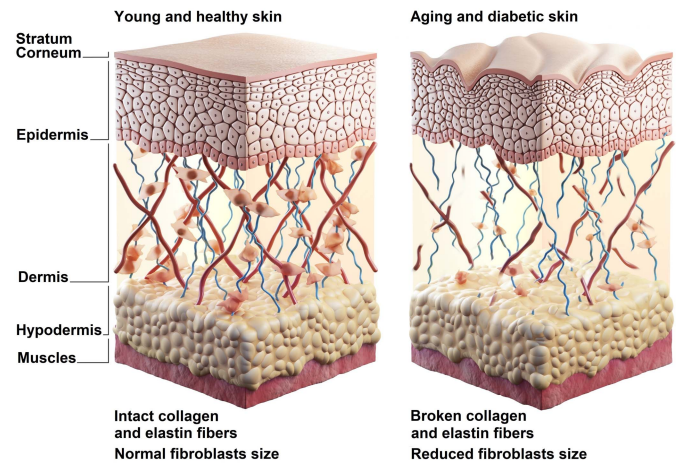

Fig. 1. Schematic illustration of the age-related and diabetic changes in human skin. Broken collagen and elastin fibers and reduced fibroblast size are the hallmarks of structural changes in aging and diabetic skin.

extremity complications due to DM [13]. Thus, the development of portable and low-cost imaging systems demonstrates a strong potential for the implementation of hyperspectral imaging technology in our everyday life and the day-to-day practice of clinicians.

However, the considered HSI techniques utilize DRS primarily for the assessment of specific tissue chromophores/absorbers concentration. In this case, the possible changes in the scattering properties caused by the alteration in the sample structure are not directly taken into account.

At the same time, changes in the structural properties of the skin are an important factor in assessing skin aging and diabetic complications. Endogenous processes in diabetes that trigger skin aging include excessive free radical production, nuclear/mitochondrial gene mutation, cellular senescence, shortening of telomere, reduced cell proliferation, and impaired immune functioning [21], [22]. In recent years, many scientific studies have revealed that advanced glycation end products (AGEs) are also among the crucial contributing factors of skin aging [21], [23], [24]. Skin aging is also associated with microstructural changes in collagen and its molecular organization [25]. Atomic force microscopy study of skin biopsy samples [26] has shown the changes in the mechanical properties of collagen in diabetes. In particular, the changes include a violation of the integrity of dermal collagen, disorganization of collagen fibrils, and nanoscale fragmentation (see the schematic illustration of the age-related and diabetic changes in human skin in the Fig. 1).

It is known that collagen is one of the main skin constituents defining its optical scattering as well as birefringent properties [27]. The magnitude of scattering and birefringence is related to the density and other mechanical properties of the collagen fibers [28]–[30]. Recent cohort studies have shown that skin aging and related collagen changes have a high inverse correlation with skin scattering properties [31], [32]. A young and healthy skin with an unfragmented collagen structure has an increased scattering coefficient in comparison to the aged skin, which leads to a decrease in the degree of the polarization of the scattered polarized light [33]. Therefore,

Fig. 2. Presented compact, hand-held hyperspectral imaging system can be easily applied for imaging in an arbitrary selected area of skin. (a) The setup has been verified in measurements of the palmar skin surface. (b) In clinical studies of DM patients, the system has been purposed for measurements in the dorsal surface of feet. (c) Flowchart of data processing. Blocks 1–3 are performed prior to the measurements. Block 4 is performed in line with the data acquisition.

the polarization of light will also be sensitive to age and structural changes in the skin. It has already been shown that the degree of residual polarization (*DOP*) is a sensitive parameter to the changes in the structure of collagen fibers [29], [34]–[36]. In particular, polarization methods were used to assess microstructural changes in biological tissues caused by cancer [37], [38], diabetes wounds [39], burns [40], [41], neurodegeneration [42], [43], etc. Thus, polarization-sensitive methods also look promising for assessing the skin condition in case of age-related and diabetic changes. Supplementary Figure 1 shows the general principle of diagnostics of structural changes in the skin, based on the registration of the parameter of the *DOP*.

Here we introduce a novel polarization-enhanced neural network-assisted hyperspectral method for monitoring blood content, blood oxygenation, and structural changes in the skin of patients with DM. To the best of our knowledge, the current work is the first one that applies hyperspectrally-resolved polarization index for *in vivo* study of diabetic patients and Monte Carlo-trained artificial neural networks for processing the hyperspectral data. Here, we perform the proof-of-concept studies for our approach and report the first clinical application of the system. Our system is ready for wide clinical use as a universal tool for label-free non-contact identification of DM complications.

II. METHODS

A. Hyperspectral Imaging System

A compact imaging system [44] (see Fig. 2a,b and Supplementary Figure 2) was built on the basis of the hyperspectral snapshot camera (Senop Optronics, Finland) utilizing a micro Fabry-Perot tunable filter providing spectral resolution of 6–10 nm within the wavelength range of 510–900 nm (see Supplementary Table 1).

A halogen broadband illumination unit is based on a fiberoptic ring illuminator (Edmund Optics, USA) providing a uniform distribution of light intensity in the camera focal plane. This ring illuminator allows to combine the lighting and detection axes. Normalized spatially-resolved reflectance was defined as a ratio of dark-noise-corrected light intensity

reflected from the skin and that reflected from the Gray Spectralon diffuse reflectance standard (50% reflection, Labsphere, Inc., USA). A data from the reflectance standard was recorded every time before the measurement of an object. In general, the developed device is capable of recording spatially and spectrally resolved light reflectance used for further artificial neural network (ANN) analysis. For a detailed description, see the Neural networks section. The developed HSI system is primarily sensitive to the variations of blood content in the papillary dermis, upper blood net plexus, and is able to cover the top part of the reticular dermis (see Supplementary Methods, Supplementary Figure 3 and Supplementary Movie 1). It is worth noting the system and data processing approach has been verified by measurements on phantoms and different ethnic skin types in Ref. 44.

In the present study, we also adapt this system to measure the degree of linear polarization (*DOLP*) of radiation reflected from a biological tissue. In general, total *DOP* can be derived from the components of the corresponding Stokes vector. However, in some cases, the determination of all elements of the Stokes vector is redundant [29] and using other polarization states would significantly complicate the system and its ability to be used in *in vivo* clinical conditions [45]–[47]. The system was equipped with a rotating linear polarizer, which can be placed either parallel or perpendicular to the initial polarization of the light source. Accounting for the *DOLP* of the light scattered from a sample significantly improves the imaging contrast between slightly different tissue structures and offers in consequence a sensitive parameter for the discriminant analysis [48]. In addition, the normalization of the difference image by the sum image cancels the variation in the illumination and the melanin effect [29]. As a diagnostic criterion, the polarization index (*PI*) is proposed in this study. *PI* represents the integrated value of *DOLP* spectrum normalized by the number of bands of the hyperspectral camera (see bellow). When measuring blood volume fraction (*BVF*) and skin blood oxygenation (*SBO*), the rotating polarizer was fixed in the crossed position in respect to the polarizer on the illumination ring for the reduction of specular reflection from the measured object.

B. Data Pre-Processing

The recorded intensity of reflectance was normalised according to:

$$I = \frac{I_{\text{tissue}} - I_{\text{dark}}}{I_{\text{spectralon}} - I_{\text{dark}}}, \tag{1}$$

where I_{tissue} is the measured diffuse reflectance in the biological tissue, $I_{\text{spectralon}}$ is the measured diffuse reflectance of the grey spectralon diffuse reflectance standard, and I_{dark} is the dark counts measured from the sensor.

For *DOLP* calculations, two normalized hyperspectral images were acquired:

$$DOLP = \frac{I_{\|} - I_{\perp}}{I_{\|} + I_{\perp}}, \tag{2}$$

where $I_{\|}$ and $I_{\perp}$ are, respectively, the backscattered intensities for parallel and perpendicular orientation of the polarizers.

The *PI* is defined from *DOLP* spectrum as:

$$PI = \frac{1}{B} \sum_{\lambda_i = \lambda_{\min}}^{\lambda_{\max}} DOLP(\lambda_i), \tag{3}$$

where $\lambda_{\min} = 510$ nm and $\lambda_{\max} = 900$ nm define the borders of the considered spectral range, and $B = 79$ is the number of spectral bands of the setup. The normalization to the spectral bands number allows one to get the average value of *DOLP* that is ranged from 0 to 1.

C. Neural Networks

Matlab R2018b Deep Learning Toolbox was adapted to build and train a set of ANN for the retrieval of skin parameters. For the training of ANN and estimation of *BVF* and *SBO*, the diffuse reflectance spectra of the skin for all possible combinations of the considered parameters were simulated by GPU-accelerated Monte Carlo technique [49], [50].

A main flowchart of data processing is demonstrated in Fig. 2c. The data processing steps can be divided into two groups. The first group consisting of the training dataset modeling and training the ANN is performed prior to the measurements. The second group is the use of the trained ANN for processing the hyperspectral measurements results and reconstruction of the target parameters. The normalization procedure was implemented in the data processing algorithm and dedicated to the mitigation of possible height variations of the skin surface in the camera field of view. The vector normalization (by L²-norm) for both the training dataset and the measured data was used to obtain the corresponding unit vectors. The detailed description of the hyperspectral system and algorithms for data processing are presented in Ref. 44 and Supplementary Methods. The developed approach is capable of close to real-time hyperspectral image processing. It should be noted that our approach provides measurement values close to the absolute values of blood volume in the tissue, the accuracy of which is determined by the developed numerical model of the skin.

D. Ethics

The healthy volunteer group was assembled through an internal university advertising campaign. According to the University of Oulu Ethics Committee regulations, informed consent was obtained from all volunteers. The clinical study protocol was approved by the local ethics committee from 03.04.2019 (protocol No. 28). All studies were conducted in accordance with the principles set out in the Helsinki Declaration of 2013 by the World Medical Association.

E. Statistics

Nonparametric Mann-Whitney U-test was used to confirm the reliability of differences in the results. Values of $p < 0.01$ were considered significant. The relationship of parameters was estimated using Pearson's correlation coefficient. A linear discriminant analysis was used to determine the discriminant function. To ensure the stability of the classifier and avoid over-fitting was used lave-one-out cross-validation. The quality of discriminant analysis was evaluated using the ROC-curve.

III. RESULTS

A. System Validation

The developed HSI system was used to perform trial measurements including the arterial and venous occlusion tests in healthy volunteers. Caucasian male skin corresponding to the type II of Fitzpatrick scale was considered. The skin surface position relative to the axis of linear polarizer of the illumination unit was fixed for the measurement of all patients and healthy volunteers. During the measurements, the axis was directed along the measured limb. At the same time, our studies have shown that the object position practically does not affect the measurement of *BVF* and *SBO*. This is achieved by orthogonal illumination and a stable distance to the object, which is controlled by the length of the lens hood. Arterial occlusion and venous occlusion tests were performed on the upper arm using a sphygmomanometer air cuff with a pressure of 200–220 mmHg and 80–100 mmHg, correspondingly. Additionally, finger occlusion test has been performed. During the finger occlusion, to suppress blood circulation and oxygenation the ring finger of the right hand was occluded with a elastic band. Hyperspectral images of the skin of the palm and fingers before the occlusion, after 3 min of continuous occlusion, and 1 min after the release of the occluded arm and ring finger were obtained. Each occlusion test was a separate measurement with a significant time interval in between to enable full tissue recovery.

In the experimental study, *BVF* and *SBO* were assessed by the developed neural network-assisted HSI method. Hyperspectral images of the inner side of the fingers and the palm were obtained (see Fig. 2a and Supplementary Figure 6). 2D distribution maps of *BVF* and *SBO* were reconstructed. The melanin content and epidermal thickness of skin have been taken into account to obtain correct values of blood fraction and oxygenation for different skin types. The epidermis thickness was fixed at the typical average thickness [51] of 100 μm.
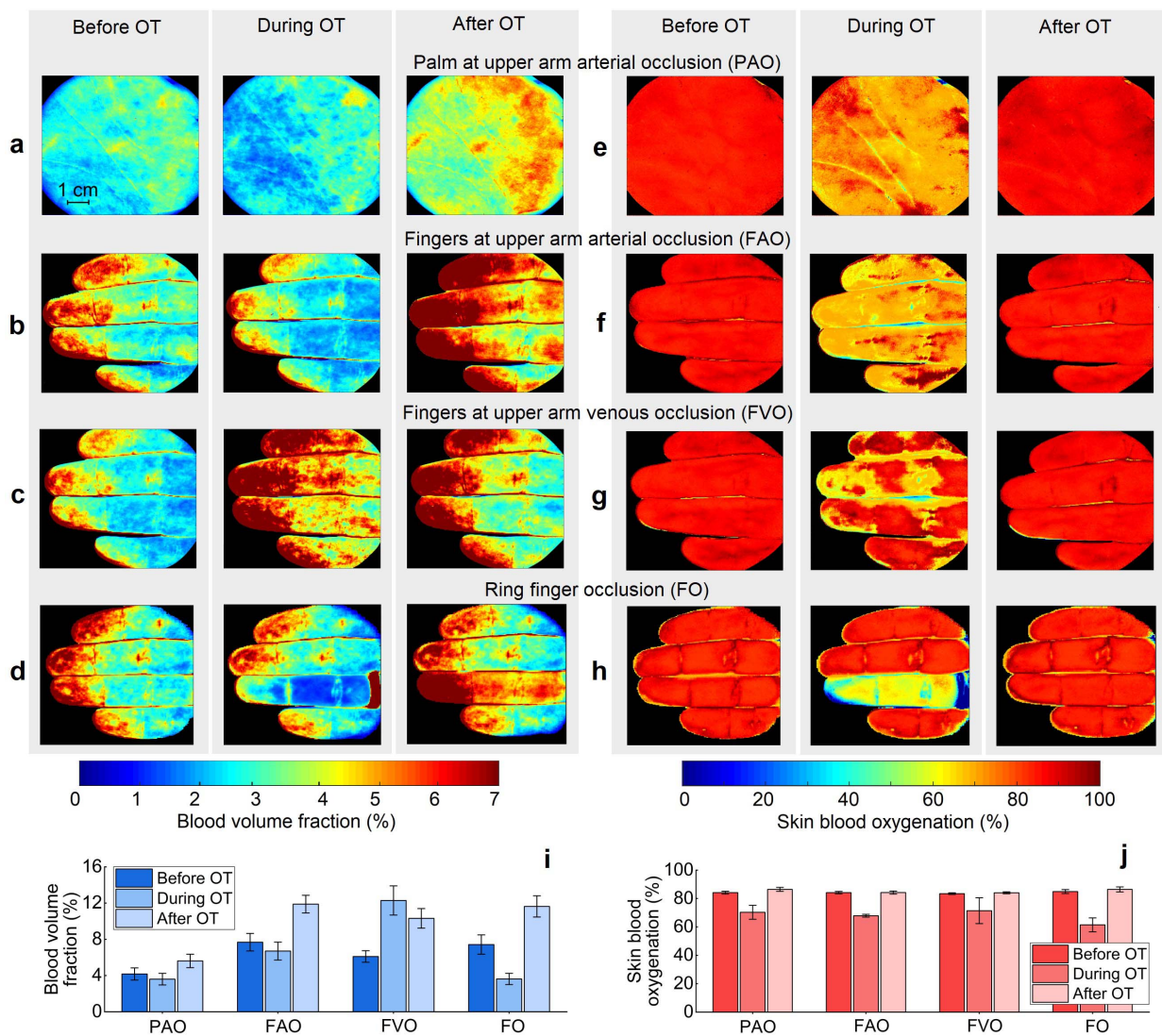
Fig. 3. Retrieved maps of *BVF* and *SBO* before, during, and 1 min after different occlusion tests indicate the high repeatability of the measuring procedure. (a) Palm with upper arm arterial occlusion. (b) Fingers with upper arm arterial occlusion. (c) Fingers with upper arm venous occlusion. (d) Fingers with arterial occlusion of one finger. (e–h) Corresponding maps of *SBO* before, during, and 1 min after different occlusion tests for the considered skin zones. (i) Mean values and standard deviation of *BVF* for each stage of occlusion. (j) Mean values and standard deviation of *SBO* for each stage of occlusion.

The average value of melanin content is 1%, which is typical for Caucasian skin.

Fig. 3a–d present the reconstructed maps of *BVF* of the palm and fingers during the different occlusion tests performed. During the arterial occlusion of the palm and fingers (Fig. 3a,b) and finger occlusion by elastic band (Fig. 3d) the significant decrease in blood content is observed. Venous occlusion (Fig. 3c) greatly increases the blood content in the fingers, which is associated with the cessation of blood outflow. When the pressure in the cuff is low, only the veins are squeezed, while maintaining the arterial blood flow. The release of the occlusion cuff or occlusion ring causes the reactive hyperemia, which leads to an increase in *BVF* parameter.

Fig. 3e–h show the distribution maps of the *SBO* parameter before, during, and after the different occlusion tests for the considered skin zones. The average *SBO* level is of 80–85% for not occluded tissues. These values correspond to the average

oxygen saturation between the arterial (95–99%) and venous (~75%) blood [52]. The 3-minute finger occlusion reduces the blood oxygen content to the level of 60–65% (Fig. 3h). More gentle arterial and venous occlusions lower the oxygenation values to 70–75% (Fig. 3e–g). It can be seen that the decrease in oxygenation in venous occlusion is more local. After the release of the occlusion, the oxygenation quickly restored to its initial value. The mean values and standard deviation of *BVF* and *SBO* for each stage of different occlusion tests are presented in Fig. 3i, j, correspondingly.

Preliminary studies of the capacity of the proposed *PI* parameter for monitoring the age-related human skin changes were also conducted. For this purpose, 32 healthy volunteers (9 males and 23 females, aged 22–76 yr) were recruited. Hyperspectral images of the skin at the parallel and perpendicular orientation of the polarizers were recorded on the palm dorsal surface. Fig. 4a–c show examples of the *PI* images for three female volunteers of different ages. A general increase
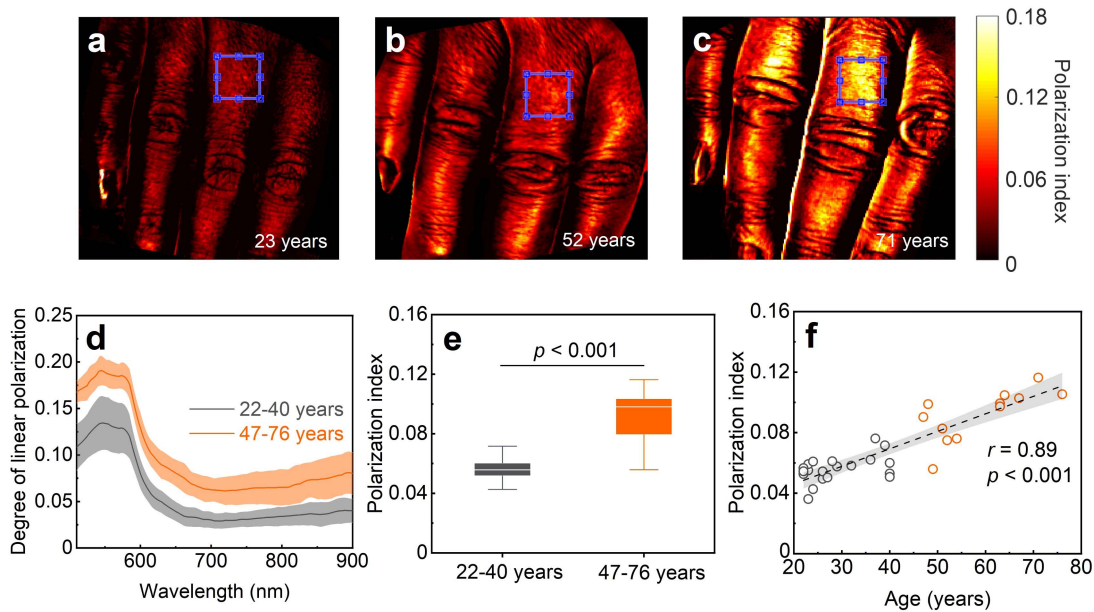
Fig. 4. Polarization sensitive hyperspectral system allows one to identify the age-specific changes. (a–c) Retrieved *PI* maps for healthy female volunteers: (a) 23 yr; (b) 52 yr; (c) 71 yr. Region of interest (blue rectangle, 8 × 8 mm) indicates the averaging area to obtain the *DOLP* spectra. (d) *DOLP* spectra for two age groups: 22–40 and 47–76 yr. (e) Comparison of *PI* among two age groups. (f) Correlation between *PI* and age (gray circle–22–40 yr; orange circle–47–76 yr, confidence level is 95%).
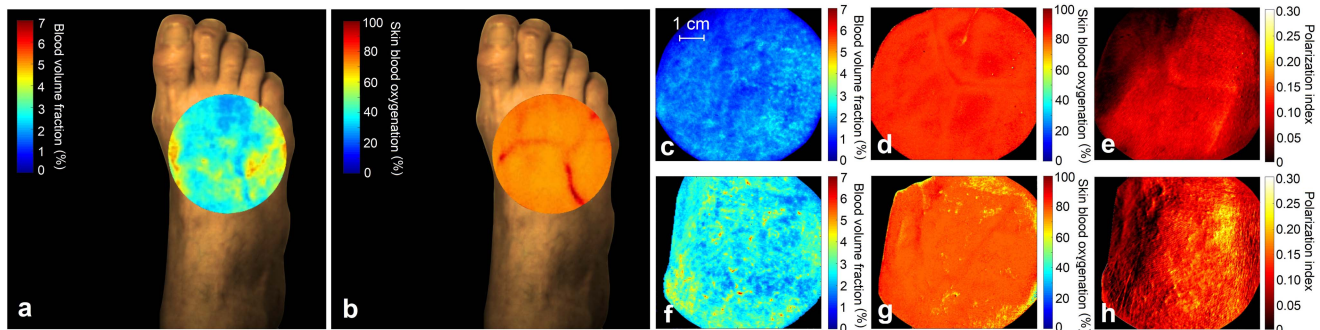

Fig. 5. The developed hyperspectral system is capable of reliably visualising the *BVF* and *SBO* parameters in the dorsal surface of feet. (a,b) FOV of the HSI system (8×8 cm^2) with the calculated parameters of (a) *BVF* and (b) *SBO*. (c-h) Typical reconstructed maps of the *BVF* (c, f), *SBO* (d, g) and *PI* (e, h) for the control (upper row, c-e) and diabetic (lower row, f-h) groups, correspondingly.

of the *PI* parameter is observed with an age. For the detailed analysis, the volunteers were divided into two age groups: 22–40 and 47–76 yr.

Fig. 4d shows the spectral distributions of the *DOLP* of radiation backscattered from skin at different ages. The spectral dependences of the *DOLP* are affected by the presence of skin absorbers (e.g., blood, melanin) and scatterers (e.g., collagen, elastin). A statistically significant increase of *PI* parameter for elderly group (47–76 yr) is observed (Fig. 4e). In particular, the average value of *PI* for this group is 76% higher than for younger volunteers (22–40 yr). Fig. 4f shows the relationship between the *PI* and the age ($r = 0.89$, $p < 0.001$, Pearson correlation). The increase can be explained by the negative correlation between the skin scattering coefficient and the human age demonstrated in Ref. 31. Specifically, a decrease in the concentration of skin collagen during aging [28] causes the decrease in the skin scattering. However, for the polarized light, the multiple scattering results in a loss of polarization. Thus, the low values of the scattering coefficient in older age lead to lower depolarization and, as a consequence, to higher values of *DOLP*. The proposed approach shows promise for *in vivo* non-invasive real-time assessment of age-related skin

changes and can be also extended to monitor the changes associated with the development of DM.

B. Clinical Study of Diabetic Patients

The experimental clinical study involved 20 patients (10 men and 10 women, mean age 54 ± 11 yr) with Caucasian skin type and with type 2 DM at the Medical Center Plavnieki and the Pauls Stradins Clinical University Hospital (Riga, Latvia). The control group consisted of 20 healthy volunteers (mean age 48 ± 14 yr). 13 participants (65%) were women. The main characteristics of the target groups are presented in Table I. The compared groups are statistically homogeneous with a difference in fasting glucose level and body mass index ($p < 0.01$, Mann-Whitney U-test).

The measurements were performed on the dorsal surface of the foot (see Fig. 2b and Supplementary Figure 6). All studies were performed in the sitting position. The study participants refrained from food and drink two hours before the study to exclude the influence of these factors on the microcirculation. Room temperature was maintained steadily at 24–25 °C.

Hyperspectral images of the dorsal surface of the foot of patients with DM were obtained. Moreover, 2D distribution

Characteristics	Diabetic group	Control group	p value
Gender, M/F	10/10	7/13	0.35, NS
Age, yr	54 ± 11	48 ± 14	0.17, NS
Systolic BP, mmHg	139 ± 19	131 ± 9	0.16, NS
Diastolic BP, mmHg	81 ± 7	79 ± 5	0.35, NS
Body mass index, kg/m^2	34.6 ± 5.8	23.2 ± 2.2	< 0.001
Fasting glucose, mmol/l	8.7 ± 3.1	4.7 ± 0.5	< 0.001
Diabetes duration, y	15 ± 10	–	–
HbA1c, %	8.3 ± 1.6	–	–
HbA1c, mmol/mol	67 ± 9	–	–
Total cholesterol, mmol/l	5.3 ± 1.2	–	–
Creatinine, μmol/l	79 ± 26	–	–
ALT, IU/L	31 ± 8	–	–
Microvascular disease, %	–	–	–
Polyneuropathy	95	–	–
Angiopathy	20	–	–
Retinophaty	45	–	–
Nephropathy	75	–	–
Stage of diabetes, %	–	–	–
Compensated	30	–	–
Subcompensated	70	–	–

Note: The data are mean $\pm$ SD unless stated otherwise. NS=not significant.
Note: Reference values of the laboratory: HbA1c 4.0% to 6.0%, total cholesterol 3.5 to 5.0 mmol/l, creatinine 70 to 110 μmol/l, and ALT 10 to 38 IU/L.

maps of *BVF* and *SBO* were reconstructed, the melanin content and the epidermal thickness of skin have been taken into account. Fig. 5a,b show the measurement area (field of view (FOV) of HSI system) with the calculated parameters of *BVF* and *SBO*, respectively. Typical distribution maps of the calculated parameters for the control and the diabetic groups are presented in Fig. 5c–h.

All parameters were averaged over the FOV of the system. Experimental studies have shown that diabetic patients have elevated values of *BVF* and *PI*, as well as a lower *SBO* level (see Fig. 6a).

The results of the computation of *BVF* show that high blood content is observed in DM patients. This can be explained by a number of factors. When venous stasis, associated with venous insufficiency characteristic of diabetic patients [53], all functioning veins become wider, and those venous vessels that had not previously functioned are open. Capillaries also expand, mainly in the venous parts. The elevated values of this parameter can also be accounted for by a blood flow to the lower limbs due to inflammation and healing processes, which can be observed in patients with DM [1]. For patients with DM, it is also necessary to take into account the presence of complex cardiovascular pathology and nephropathy, which can lead to variations in blood content.

The obtained data on understated tissue saturation in diabetics in comparison with the control group match those previously obtained by other studies [54]–[56]. It is known that hyperglycemia may increase oxygen consumption in mitochondria, resulting in cellular hypoxia [57], [58]. In this regard, the retrieval of blood content and oxygen saturation can be useful in the study of blood stasis, leading to edema

and trophic disorders, as well as in monitoring therapeutic procedures aimed at healing trophic ulcers.

Fig. 6b shows the averaged spectra of *DOLP* for control and diabetes groups with the difference in the entire wavelength range. It should be noted that the spectral dependences of the *DOLP* reflect the presence of blood in the skin tissue (an increase in the *DOLP* in the spectral bands of hemoglobin absorption) [59]. In this regard, to assess the influence of blood content on the difference in the spectra, the dependence of *PI* from *BVF* was plotted. As can be seen from Fig. 6c there is no statistically significant correlation between these parameters. We assume that it is the presence of diabetes and associated skin changes that affect the difference in *DOLP* spectra.

Considering the connection of diabetic changes and aging processes [1], [21], we assume that the presence of DM as well as aging reduces the loss of polarization. Additionally, we checked the relationship between *PI* and age for the diabetic group. As can be seen from the Fig. 6d, there is also no correlation between these parameters. This confirms the assumption that the presence of diabetes is the main factor affecting the polarization properties of patients' skin.

The analysed parameters (*BVF*, *SBO*, and *PI*) were used for the synthesis of the decision rule. These parameters satisfy the principles of statistical independence and the significance of the differences of their values, calculated for the patients' and control groups (see Fig. 6a). Table II summarises the sensitivity, specificity, and area under the curve (AUC) for a different combination of measured parameters. As can be seen from the table, the combination of all three parameters provides the highest sensitivity and specificity values.
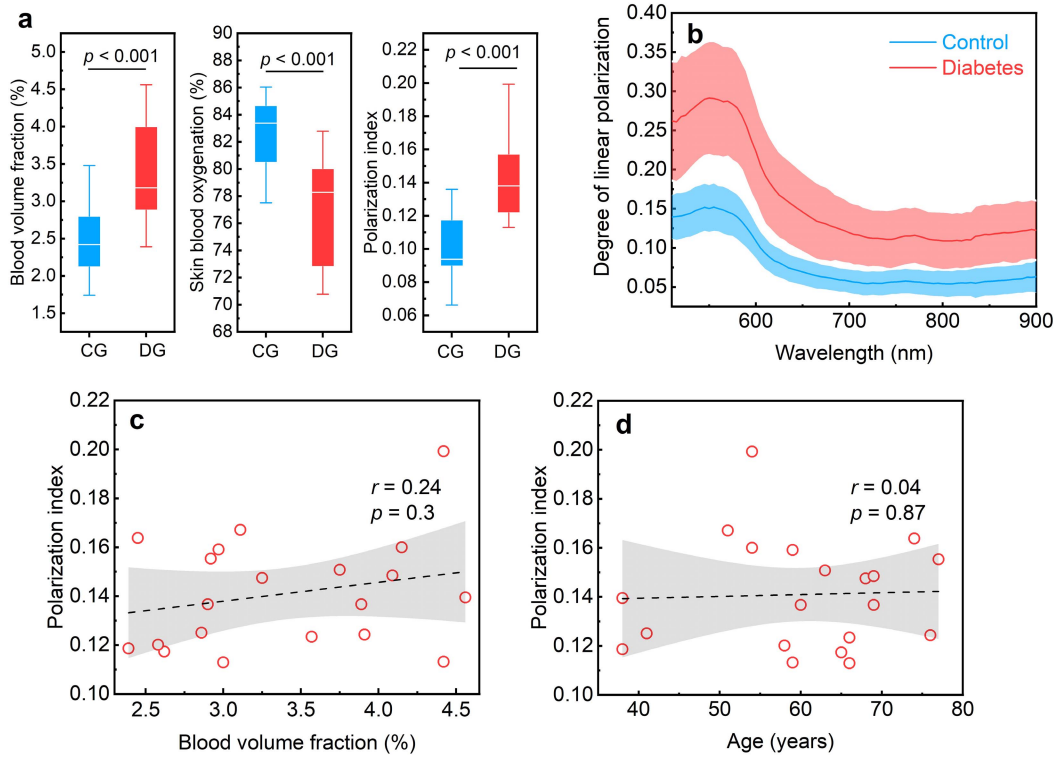
Fig. 6. The parameters of *BVF*, *SBO*, and *PI* were found to have statistically significant difference between the control and the diabetic groups. (a) Comparison of parameters between control (CG, blue bars) and diabetic (DG, red bars) groups. The box central line is the median of the group, the edges are the 25th and 75th percentiles. (b) Mean spectral dependences of the *DOLP* (solid line) and standard deviation for two groups: control (blue line) and diabetes (red line). (c,d) Correlation between (c) PI and BVF and between (d) PI and age for diabetes group (confidence level is 95%).

TABLE II
SENSITIVITY, SPECIFICITY, AND AUC FOR THE CLASSIFICATION RULE

Parameter	BVF, SBO	BVF, PI	SBO, PI	BVF, SBO, PI
Sensitivity	0.85	0.80	0.95	0.95
Specificity	0.80	0.80	0.80	0.85
AUC	0.94	0.93	0.96	0.97

Fig. 7a shows the 3D scatter plot of experimental data with the applied discriminant surface that divides the experimental points into two groups with better combination of sensitivity and specificity. The phenomenological diagnostic criterion in the form of discriminant functions (*D*) allows for attributing a newly measured subject to one of the two groups:

$$D = 8.9 + 0.5BVF - 0.2SBO + 28.9PI. \qquad (4)$$

The ROC-curves and integral characteristic of AUC were calculated for the obtained discriminant functions (see Fig. 7b and Table II).

IV. DISCUSSION

The developed hyperspectral system has shown the ability to sense the alterations of blood content, blood oxygenation, and collagen structure in human skin *in vivo*. The implementation of the ANN-based processing allows for fast recovery of the considered skin parameters. Our concept was successfully demonstrated in preclinical experiments and clinical studies

and satisfied the major requirements for modern medical imaging techniques by providing: high FOV, high spectral resolution, close to real-time data acquisition and processing, high level of sensitivity and specificity.

This is the first *in vivo* human clinical study to report a label-free, non-invasive polarization-sensitive approach that can discriminate between the skin of DM patients and control participants. We showed that polarization-enhanced hyperspectral analysis can differentiate the skin tissue with age-related and DM changes. We assume that the shown differences in the *PI* parameter, characterizing the age-related collagen changes, can form the basis for the diagnosis of DM complications. Prediction of ulcers can also be based on the detection of changes in collagen structure. Fig. 6d shows the absence of correlation between the age of the patients with diabetes and *PI*. In the same time, a significant correlation is observed for the control group of healthy volunteers. It can be explained by the fact that the presence of diabetes can distort the collagen structure at any age and thus hinders the dependence of *PI* on the age for diabetic group. That, in particular, supports our suggestion of the sensitivity of *PI* to the changes in collagen structure that is altered in the presence of diabetes (Fig. 6a). It should be borne in mind that the blood content in the biotissue, epidermis thickness, and some other factors may specifically affect the residual polarization spectra. Thus, hyperspectral polarization imaging, in contrast to the standard approach with the registration of reflected light, allows for more detailed tissue analysis, including selectively tracking changes in the concentration of various absorbers and scatterers in the biotissue.
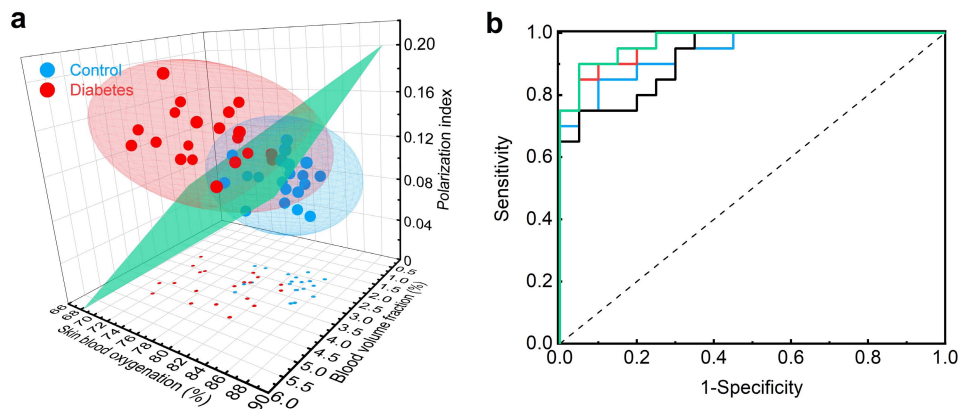
Fig. 7. The simultaneously measured values of *BVF, SBO, PI* underlies the set of developed diagnostic classifiers of high sensitivity and specificity. (a) The 3D scatter plot and the decision surface for a three-dimensional LDA classifier. 3D ellipsoids are confidence regions (confidence level is 95%). (b) ROC curves for assessing the effectiveness of the classifiers. The healthy group is shown by blue circles, the diabetic group by red circles. For the ROC analysis: blue line denotes *BVF, SBO*, black line – *BVF, PI*, red line – *SBO, PI*, green line – *BVF, SBO, PI*.

Nonetheless, for future clinical applications, our technique can be improved and expanded. The developed data processing algorithm allows almost real-time processing of the hyperspectral images, however, the time of the hypercube acquisition and the duration of the data transfer via USB port impose the main limitation on the system performance. The hyperspectral sensor with specific spectral resolution and wavelength range could be flexibly optimised according to application requirements. In this study, a spectral band of 510–900 nm was utilized. However, the application of a sensor with an extended spectral range up to 1000 nm may provide an additional possibility to analyze the content of water and fat in tissues. Additionally, the use of UV or blue sources in the lighting channel will allow the HSI method to be used for the fluorescence analysis of AGEs, as well as the respiratory chain coenzymes NADH and FAD [60], [61]. There is also further potential to expand the number of clinical investigations that will eventually allow the methods in question to be introduced into the practice of the attending physician.

In summary, we have developed a compact HSI system utilizing ANN-based processing approach for the calculation of distribution maps of skin blood content, blood oxygenation, and the polarization index of the reflected radiation. The proposed system is capable of close to real-time hyperspectral image processing. The use of polarization-sensitive hyperspectral imaging and parameters of *BVF*, *SBO*, and *PI* in combination or individually can have important clinical applications since they can help to identify patients with different degrees of microcirculation impairments in the lower extremities. The proposed parameters could serve as biomarkers of diabetic complications. They can also be used to evaluate therapeutic procedures aimed at preventing or reversing diabetic complications. Employment of the *PI* parameter increases the sensitivity and specificity of the method up to the level of 95% and 85%, respectively, compared to the approach that relies only on *BVF* and *SBO* (sensitivity 85%, specificity 80%). Our results can facilitate the development of the HIS technique and give a new direction in the studies of age-related diseases.

REFERENCES

[1] *IDF Diabetes Atlas. 9th Ed.*, Int. Diabetes Fed., Brussels, Belgium, 2019.

[2] P. Zhang, J. Lu, Y. Jing, S. Tang, D. Zhu, and Y. Bi, "Global epidemiology of diabetic foot ulceration: A systematic review and meta-analysis," *Ann. Med.*, vol. 49, no. 2, pp. 106–116, Feb. 2017.

[3] W. D. Strain and P. M. Paldánius, "Diabetes, cardiovascular disease and the microcirculation," *Cardiovascular Diabetol.*, vol. 17, no. 1, p. 57, Dec. 2018.

[4] D. B. Schmolze, C. Standley, K. E. Fogarty, and A. H. Fischer, "Advances in microscopy techniques," *Arch. Pathol. Lab. Med.*, vol. 135, no. 2, pp. 255–263, 2011.

[5] Y. Sun and N. Thakor, "Photoplethysmography revisited: From contact to noncontact, from point to imaging," *IEEE Trans. Biomed. Eng.*, vol. 63, no. 3, pp. 463–477, Mar. 2016.

[6] E. A. Swanson and J. G. Fujimoto, "The ecosystem that powered the translation of OCT from fundamental research to clinical and commercial impact," *Biomed. Opt. Exp.*, vol. 8, no. 3, pp. 1638–1664, Mar. 2017.

[7] Z. Hu *et al.*, "First-in-human liver-tumour surgery guided by multispectral fluorescence imaging in the visible and near-infrared-I/II windows," *Nature Biomed. Eng.*, vol. 4, no. 3, pp. 259–271, Mar. 2020.

[8] Y. P. Sinichkin, N. Kollias, G. I. Zonios, S. R. Utz, and V. V. Tuchin, "Reflectance and fluorescence spectroscopy of human skin *in vivo*," in *Handbook of Optical Biomedical Diagnostics*, 2nd ed., vol. 2. Bellingham, WA, USA: SPIE, 2017, pp. 99–198.

[9] L. Zhang *et al.*, "Light scattering spectroscopy identifies the malignant potential of pancreatic cysts during endoscopy," *Nature Biomed. Eng.*, vol. 1, no. 4, p. 0040, Apr. 2017.

[10] L. Qiu *et al.*, "Multispectral light scattering endoscopic imaging of esophageal precancer," *Light, Sci. Appl.*, vol. 7, no. 4, p. 17174, 2018.

[11] E. J. M. Baltussen *et al.*, "Diffuse reflectance spectroscopy as a tool for real-time tissue assessment during colorectal cancer surgery," *J. Biomed. Opt.*, vol. 22, no. 10, 2017, Art. no. 106014.

[12] Y. Zhang *et al.*, "Physiological model using diffuse reflectance spectroscopy for nonmelanoma skin cancer diagnosis," *J. Biophotonics*, vol. 12, no. 12, Dec. 2019, Art. no. e201900154.

[13] E. Zharkikh, V. Dremin, E. Zherebtsov, A. Dunaev, and I. Meglinski, "Biophotonics methods for functional monitoring of complications of diabetes mellitus," *J. Biophotonics*, vol. 13, no. 10, Oct. 2020, Art. no. e202000203.

[14] J. Yoon *et al.*, "A clinically translatable hyperspectral endoscopy (HySE) system for imaging the gastrointestinal tract," *Nature Commun.*, vol. 10, no. 1, pp. 1–13, Dec. 2019.

[15] G. Lu and B. Fei, "Medical hyperspectral imaging: A review," *J. Biomed. Opt.*, vol. 19, no. 1, pp. 1–24, 2014.

[16] D. W. Paul *et al.*, "Noninvasive imaging technologies for cutaneous wound assessment: A review," *Wound Repair Regener.*, vol. 23, no. 2, pp. 149–162, Mar. 2015.

[17] C. G. Ross, C. Chwal, J. A. Beckstead, R. W. Byard, and N. E. I. Langlois, "Hyperspectral imaging of bruises," *Pathology*, vol. 46, no. Suppl. 1, p. S88, 2014.

[18] D. Yudovsky, A. Nouvong, K. Schomacker, and L. Pilon, "Assessing diabetic foot ulcer development risk with hyperspectral tissue oximetry," *J. Biomed. Opt.*, vol. 16, no. 2, 2011, Art. no. 026009.

[19] L. Khaodhiar *et al.*, "The use of medical hyperspectral technology to evaluate microcirculatory changes in diabetic foot ulcers and to predict clinical outcomes," *Diabetes Care*, vol. 30, no. 4, pp. 903–910, Apr. 2007.

[20] A. Nouvong, B. Hoogwerf, E. Mohler, B. Davis, A. Tajaddini, and E. Medenilla, "Evaluation of diabetic foot ulcer healing with hyperspectral imaging of oxyhemoglobin and deoxyhemoglobin," *Diabetes Care*, vol. 32, no. 11, pp. 2056–2061, Nov. 2009.

[21] P. Gkogkolou and M. Böhm, "Advanced glycation end products: Key players in skin aging?" *Dermato-Endocrinol.*, vol. 4, no. 3, pp. 259–270, Jul. 2012.

[22] Y. Tu and T. Quan, "Oxidative stress and human skin connective tissue aging," *Cosmetics*, vol. 3, no. 3, p. 28, Aug. 2016.

[23] S. F. Yan, R. Ramasamy, and A. M. Schmidt, "Mechanisms of disease: Advanced glycation end-products and their receptor in inflammation and diabetes complications," *Nature Clin. Pract. Endocrinol. Metabolism*, vol. 4, no. 5, pp. 285–293, May 2008.

[24] S.-Y. Goh and M. E. Cooper, "The role of advanced glycation end products in progression and complications of diabetes," *J. Clin. Endocrinol. Metab.*, vol. 93, no. 4, pp. 1143–1152, 2008.

[25] S. Bansode *et al.*, "Glycation changes molecular organization and charge distribution in type i collagen fibrils," *Sci. Rep.*, vol. 10, no. 1, pp. 1–13, Dec. 2020.

[26] A. J. Argyropoulos *et al.*, "Alterations of dermal connective tissue collagen in diabetes: Molecular basis of aged-appearing skin," *PLoS ONE*, vol. 11, no. 4, Apr. 2016, Art. no. e0153806.

[27] R. Puxkandl *et al.*, "Viscoelastic properties of collagen: Synchrotron radiation investigations and structural model," *Phil. Trans. Roy. Soc. London B, Biol. Sci.*, vol. 357, no. 1418, pp. 191–197, Feb. 2002.

[28] S. Shuster, M. M. Black, and E. McVitie, "The influence of age and sex on skin thickness, skin collagen and density," *Brit. J. Dermatol.*, vol. 93, no. 6, pp. 639–643, Dec. 1975.

[29] V. V. Tuchin, "Polarized light interaction with tissues," *J. Biomed. Opt.*, vol. 21, no. 7, Apr. 2016, Art. no. 071114.

[30] S. J. Matcher, "A review of some recent developments in polarization-sensitive optical imaging techniques for the study of articular cartilage," *J. Appl. Phys.*, vol. 105, no. 10, May 2009, Art. no. 102041.

[31] H. Jonasson, I. Fredriksson, S. Bergstrand, C. J. Östgren, M. Larsson, and T. Strömberg, "*In vivo* characterization of light scattering properties of human skin in the 475-to 850-nm wavelength range in a Swedish cohort," *J. Biomed. Opt.*, vol. 23, no. 12, p. 121608, 2018.

[32] T. Kono and J. Yamada, "*In vivo* measurement of optical properties of human skin for 450–800 nm and 950–1600 nm wavelengths," *Int. J. Thermophys.*, vol. 40, no. 5, p. 51, May 2019.

[33] X. Wang, L. V. Wang, C.-W. Sun, and C. C. Yang, "Polarized light propagation through scattering media: Time-resolved Monte Carlo simulations and experiments," *J. Biomed. Opt.*, vol. 8, no. 4, pp. 608–617, 2003.

[34] S. L. Jacques, J. C. Ramella-Roman, and K. Lee, "Imaging skin pathology with polarized light," *J. Biomed. Opt.*, vol. 7, no. 3, pp. 329–340, Jul. 2002.

[35] X. Feng, R. Patel, and A. N. Yaroslavsky, "Wavelength optimized cross-polarized wide-field imaging for noninvasive and rapid evaluation of dermal structures," *J. Biophotonics*, vol. 8, no. 4, pp. 324–331, Apr. 2015.

[36] X. Feng, S. Doherty, I. Yaroslavsky, G. Altshuler, and A. N. Yaroslavsky, "Polarization enhanced wide-field imaging for evaluating dermal changes caused by non-ablative fractional laser treatment," *Lasers Surgery Med.*, vol. 48, no. 2, pp. 150–156, Feb. 2016.

[37] R. Patel, A. Khan, R. Quinlan, and A. N. Yaroslavsky, "Polarization-sensitive multimodal imaging for detecting breast cancer," *Cancer Res.*, vol. 74, no. 17, pp. 4685–4693, Sep. 2014.

[38] K. Korotkov, J. Quintana, S. Puig, J. Malvehy, and R. Garcia, "A new total body scanning system for automatic change detection in multiple pigmented skin lesions," *IEEE Trans. Med. Imag.*, vol. 34, no. 1, pp. 317–338, Jan. 2015.

[39] A. E. Woessner, J. D. McGee, J. D. Jones, and K. P. Quinn, "Characterizing differences in the collagen fiber organization of skin wounds using quantitative polarized light imaging," *Wound Repair Regener.*, vol. 27, no. 6, pp. 711–714, Nov. 2019.

[40] O. Goertz *et al.*, "Orthogonal polarization spectral imaging: A tool for assessing burn depths?" *Ann. Plastic Surg.*, vol. 64, no. 2, pp. 217–221, Feb. 2010.

[41] K. H. Kim *et al.*, "*In vivo* imaging of human burn injuries with polarization-sensitive optical coherence tomography," *J. Biomed. Opt.*, vol. 17, no. 6, 2012, Art. no. 066012.

[42] B. Baumann *et al.*, "Visualization of neuritic plaques in Alzheimer's disease by polarization-sensitive optical coherence microscopy," *Sci. Rep.*, vol. 7, no. 1, p. 43477, Apr. 2017.

[43] R. Camacho *et al.*, "2D polarization imaging as a low-cost fluorescence method to detect α-synuclein aggregation *ex vivo* in models of Parkinson's disease," *Commun. Biol.*, vol. 1, no. 1, p. 157, Dec. 2018.

[44] E. Zherebtsov, V. Dremin, A. Popov, A. Doronin, D. Kurakina, M. Kirillin, I. Meglinski, and A. Bykov, "Hyperspectral imaging of human skin aided by artificial neural networks," *Biomed. Opt. Exp.*, vol. 10, no. 7, pp. 3545–3559, 2019.

[45] B. Kunnen, C. Macdonald, A. Doronin, S. Jacques, M. Eccles, and I. Meglinski, "Application of circularly polarized light for non-invasive diagnosis of cancerous tissues and turbid tissue-like scattering media," *J. Biophotonics*, vol. 8, no. 4, pp. 317–323, Apr. 2015.

[46] D. Ivanov *et al.*, "Colon cancer detection by using Poincaré sphere and 2D polarimetric mapping of *ex vivo* colon samples," *J. Biophotonics*, vol. 13, no. 8, Aug. 2020, Art. no. e202000082.

[47] P. Schucht *et al.*, "Visualization of white matter fiber tracts of brain tissue sections with wide-field imaging Mueller polarimetry," *IEEE Trans. Med. Imag.*, vol. 39, no. 12, pp. 4376–4382, Dec. 2020.

[48] A. Pierangelo *et al.*, "*Ex-vivo* characterization of human colon cancer by Mueller polarimetric imaging," *Opt. Exp.*, vol. 19, no. 2, p. 1582, 2011.

[49] V. Dremin, E. Zherebtsov, A. Bykov, A. Popov, A. Doronin, and I. Meglinski, "Influence of blood pulsation on diagnostic volume in pulse oximetry and photoplethysmography measurements," *Appl. Opt.*, vol. 58, no. 34, pp. 9398–9405, 2019.

[50] A. Doronin and I. Meglinski, "Online object oriented Monte Carlo computational tool for the needs of biomedical optics," *Biomed. Opt. Exp.*, vol. 2, no. 9, pp. 2461–2469, 2011.

[51] T. Gambichler, R. Matip, G. Moussa, P. Altmeyer, and K. Hoffmann, "*In vivo* data of epidermal thickness evaluated by optical coherence tomography: Effects of age, gender, skin type, and anatomic site," *J. Dermatol. Sci.*, vol. 44, no. 3, pp. 145–152, Dec. 2006.

[52] K. Akons, E. Dann, and D. Yelin, "Measuring blood oxygen saturation along a capillary vessel in human," *Biomed. Opt. Exp.*, vol. 8, no. 11, pp. 5342–5348, 2017.

[53] V. Fejfarová *et al.*, "The relationship between chronic venous insufficiency and diabetes mellitus," *Int. Angiol.*, vol. 36, no. 1, pp. 90–91, 2017.

[54] L. Xi, C.-M. Chow, and X. Kong, "Role of tissue and systemic hypoxia in obesity and type 2 diabetes," *J. Diabetes Res.*, vol. 2016, Jun. 2016, Art. no. 1527852.

[55] J. Ditzel and E. Standl, "The problem of tissue oxygenation in diabetes mellitus," *Acta Med. Scand. Suppl.*, vol. 578, no. S578, pp. 59–68, 1975.

[56] R. L. Greenman *et al.*, "Early changes in the skin microcirculation and muscle metabolism of the diabetic foot," *Lancet*, vol. 366, no. 9498, pp. 1711–1717, Nov. 2005.

[57] J. R. Nyengaard, Y. Ido, C. Kilo, and J. R. Williamson, "Interactions between hyperglycemia and hypoxia," *Diabetes*, vol. 53, no. 11, pp. 2931–2938, 2004.

[58] K. Sada *et al.*, "Hyperglycemia induces cellular hypoxia through production of mitochondrial ROS followed by suppression of Aquaporin-1," *PLoS ONE*, vol. 11, no. 7, Jul. 2016, Art. no. e0158619.

[59] V. V. Tuchin, L. V. Wang, and D. A. Zimnyakov, *Optical Polarization in Biomedical Applications*. Berlin, Germany: Springer, 2006.

[60] V. Dremin *et al.*, "Multimodal optical measurement for study of lower limb tissue viability in patients with diabetes mellitus," *J. Biomed. Opt.*, vol. 22, no. 8, 2017, Art. no. 085003.

[61] F. Bartolome and A. Y. Abramov, "Measurement of mitochondrial NADH and FAD autofluorescence in live cells," *Methods Mol. Biol.*, vol. 1264, pp. 263–270, Jan. 2015.